

Effect of Flow Rates on erosion corrosion behavior of hull steel in real seawater

Jiangmin Xia^{1,*}, Zhuying Li¹, Jingchao Jiang², Xiaoqiang Wang¹, Xiaodong Zhang¹

¹ College of Naval Architecture & Ocean Engineering, Naval University of Engineering, Wuhan 430033, China

² Department of Mechanical Engineering, University of Auckland, Auckland 1010, New Zealand

*E-mail: x_jiangmin@163.com

Received: 20 January 2021 / *Accepted:* 11 March 2021 / *Published:* 31 March 2021

Currently, researches on erosion corrosion were mainly focused on laboratory or computer simulation based, which were more or less different from the real environment. And most of studies only paid attention to the initial changes in a short period of the erosion corrosion process, little attention had been paid to the variation of the whole test period. Most importantly, few articles can be found to study the critical flow rate of hull steel. Therefore, in this paper, the erosion corrosion of hull steel in different flow rates were comprehensively studied in a seawater (from East China Sea) environment. The critical flow velocity for hull steel material was obtained after the first analysis. The experiments of erosion corrosion behavior had been observed for 30 days, with seawater flow rates of 0, 2, 4 and 6 m/s in a self-designed rotary scouring test platform. In order to obtain good results, all the experiments had been last for more than 30 days. Electrochemical impedance spectroscopy (Hereinafter abbreviated to EIS), Electrochemical noise (Hereinafter abbreviated to EN) and Scanning Electron Microscope (Hereinafter abbreviated to SEM) method were used to analyze the process results and then comprehensively determined the critical flow velocity. The results showed that the higher the flow rate, the more complex the erosion corrosion reacted. During these 30 days, electrochemical corrosion rate rapidly increased, and then slowed down to a stable situation as time pass by. Among these results, the flow rate of 2 m/s had the fastest electrochemical corrosion rate. Electrochemical noise average potential increased and the power spectral density (Hereinafter abbreviated to PSD) curve gradually diverges with the increase of the flow velocity, the 2 m/s flow rate electrochemical noise potential standard deviation and the white noise level had the largest value and fluctuation. As the flow rate increased, double-layer corrosion products generated; the outer corrosion products became thinner and the inner layer of corrosion products gradually formed. The corrosion product morphology at static was similar to cauliflower, while the morphologies at 4 m/s and 6 m/s flow rate were net-like; and the morphology at 2 m/s flow rate was in a situation between them. The critical synergy velocity of hull steel erosion in the East China Sea was 2 m/s after comprehensive analysis. In the future, this critical flow rate should be considered as an important operation parameter, it was best for the ship and pipe to avoid running at this speed.

Keywords: Erosion corrosion; Hull steel; Corrosion mechanism; Critical velocity.

1. INTRODUCTION

Metal materials are prone to erosion corrosion under seawater scouring. This type of corrosion is very common in ship shells and seawater pipelines, accounting for more than 5% of metal wear [1]. Scour corrosion is the phenomenon of metal damage caused by high-speed relative motion between metal surface and corrosive fluid. It is the result of mechanical and electrochemical corrosion interaction [2,3]. The weight loss of metal material caused by erosion corrosion is much greater than mechanical wear or electrochemical corrosion effect alone [4,5]. Mechanical wear plays a major role in the erosion of metals [6], while electrochemical corrosion plays an important role in the corrosion process. The main factors affecting the corrosion rate includes liquid flow rate [7-8], fluid sediment concentration [9], fluid particle size [10], fluid wash angle [11-13], fluid temperature [14], fluid pH value [15], the composition and microstructure of the material [16-18], and the heat treatment method [19].

Presently, researches on erosion corrosion mainly use laboratory simulation and seawater hanging test methods [20,21]. In literature, researchers used the weight loss method, electrochemical impedance spectroscopy and microscopic characterization to study the corrosion of metal materials in different fluid mechanics conditions, environmental factors and material properties [22-24]. In recent years, with the aim of reducing test time, cost and improving efficiency, researchers had begun to apply computer software modeling methods to simulate erosion corrosion processes [25,26]. These computer modeling approaches can help reveal the influence of fluid mechanics on erosion corrosion and finally achieve a way to reduce metal scouring corrosion in fluids [27]. Besides, the above laboratory studies mostly used artificial seawater, which was more or less different from the real environment in the sea. In a real sea environment, the seawater coupon test cannot accurately control the flow velocity. In addition, current analysis was only focused on the initial changes in a short time or focused on the comparison between pre-test and post-test, little attention had been paid to the variation of the whole test period [28,29]. For the computer simulation methods, boundary conditions were generally complex which need to be simplified. Also, these boundary conditions were different from the real environment and there was a certain gap between them. The computer modelling methods can reveal some general laws [30], but it was difficult to observe the microscopic changes in the entire erosion process [31,32].

Erosion corrosion was the result of the interaction between fluid mechanical wear and electrochemical corrosion. When the metal was washed and corroded in a corrosive solution under certain conditions, there was a critical flow velocity that led to the highest erosion corrosion synergy rate. Therefore, it was significant for protecting material from erosion corrosion to obtain and study this critical flow velocity. However, currently, there were no research articles about the critical flow velocity of hull steel material. In this paper, electrochemical corrosion performance of hull steel, as well as the microscopic test analysis of surface structure and phase composition, will be analyzed. The erosion corrosion characteristics of hull steel duration a 30-day test at different flow rates would be studied. Finally, the critical flow velocity of hull steel material would be revealed.

2. EXPERIMENTS

In this study, the erosion corrosion tests were performed at a self-designed rotary erosion corrosion test platform, as shown in Fig. 1. The experimental setup consists of four parts: a temperature

control system, a rotating disc system, a motor system and an electrochemical test system. The temperature was controlled by the temperature control system in the test tank through a heating pipe and a thermometer. The electrode was mounted on the side of the rotating disc, the electrode surface as the tangential direction of the rotating disc, and the tangential speed was the relative flushing speed of the metal and the seawater. The rotating disc can hold 4 electrodes for one time, one of the electrodes was connected to the carbon brush through the rotating disc used for electrochemical testing such as electrochemical noise and electrochemical impedance spectroscopy; the other three electrodes were used to observe the electrode surface morphology and analyze the corrosion products after different etching times. The motor system included a gearbox, a motor, a frequency converter, control the rotational and the tangential speed of the rotating disk. The electrochemical test system includes a test system consisting of a working electrode, a Pt auxiliary electrode and a reference electrode. During the experiment, the speed required for the experiment was controlled by adjusting the reduction gearbox and the frequency converter. All electrochemical tests were conducted when the scouring had reached to the corresponding time, then the motor stopped working. This can prevent the electrical signal from being disturbed by the fluid flow and make sure the measured data more accurate.

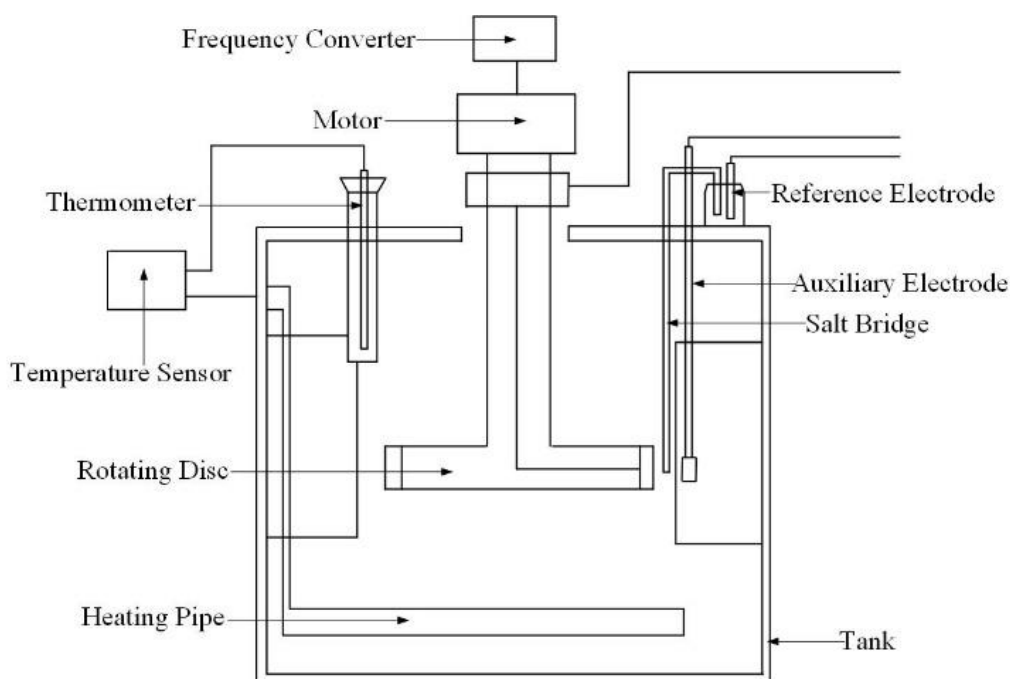


Figure 1. Experimental set-up for erosion corrosion

The electrochemical impedance spectroscopy test was performed at CS350. The electrode adopted three-electrode system. The hull steel was the working electrode, the platinum wire around the working electrode was used as the auxiliary electrode, and the saturated calomel electrode(SCE) was used as the reference electrode. The test was performed in open-circuit potential status. The amplitude of the AC excitation signal was 5 mV, the test frequency range is 100kHz~10mHz, and the sweep frequency was from high frequency to low frequency.

The electrochemical noise test was measured at a four-channel electrochemical noise meter provided by e-DAQ and used three-electrode system. The working electrode was hull steel and the auxiliary electrode was a multi-channel platinum wire around the working electrode. The saturated calomel electrode was used as the reference electrode. For noise test, a constant current mode was used to acquire 4 data points per second, with 10 Hz low pass and DC high pass.

After scouring for a certain period of time, the electrode was rinsed with the double distilled water, then blown dry, and the morphology of the corrosion product was characterized by SEM. The surface of the sample was sprayed with gold before the product was characterized by SEM. The corrosion test solution was real seawater from the East China Sea. The material used for all tests in this paper was hull steel. Table 1 showed the composition of the hull steel.

Table 1. Chemical compositions of hull Steel

Composition	C	Si	Mn	P	S	Ni	Cr	Cu	Ti
Steel	0.12	0.79	1.01	0.016	0.007	0.67	0.64	0.42	0.005

3. RESULTS AND ANALYSIS

3.1 Erosion corrosion mechanism

During the erosion corrosion of metals, the fluid flow rate played an important role in affecting the entire mass transfer process [33]. There was a critical flow rate when metal erosion corrosion occurred under certain conditions in corrosive solution. Below the critical flow rate, electrochemical corrosion dominates the entire erosion process [34]. The erosion corrosion was mainly controlled by the electrochemical corrosion mechanism. Above the critical flow rate, the metal erosion was controlled by the electrochemical corrosion and erosion wear mechanism [35]. According to the existing erosion corrosion theory, the erosion corrosion rate K_{EC} can be expressed as [36,37]:

$$K_{EC} = K_{CO} + \Delta K_C + \Delta K_E + K_{EO} \quad (1)$$

K_{CO} and K_{EO} determined by measuring are the individual electrochemical corrosion rate and the separate erosion wear corrosion rate, ΔK_C and ΔK_E were the enhancement of the electrochemical corrosion by the erosion wear and the enhancement of the wear erosion by the electrochemical corrosion. When the flow rate of the corrosive medium was the critical flow rate, the synergistic effect of erosion wear and electrochemical corrosion was the strongest, that was the maximum $\Delta K_C + \Delta K_E$ value. In general, K_{CO} was determined by measuring the short-term corrosion rate of the metal material in the static conditions, and K_{EO} was determined by measuring the short-term flushing wear rate after the cathodic protection was applied to the electrode [38].

However, the short-term corrosion rate of the metal material in the static condition was not equivalent to the single electrochemical corrosion rate when the erosion corrosion occurred; the surface roughness of the metal changes with the length of the corrosion time, and the erosion wear rate obtained

by the short-term test was not equal to the rate of erosion wear throughout the process. Therefore, the contribution of erosion wear and electrochemical corrosion to the entire corrosion was not the same. The rate calculated by the erosion corrosion rate formula was somewhat different from the actual and cannot represent the erosion corrosion rate throughout the process. It was necessary to use more diverse methods to study the erosion corrosion characteristics during the testing.

3.2 Electrochemical impedance spectroscopy

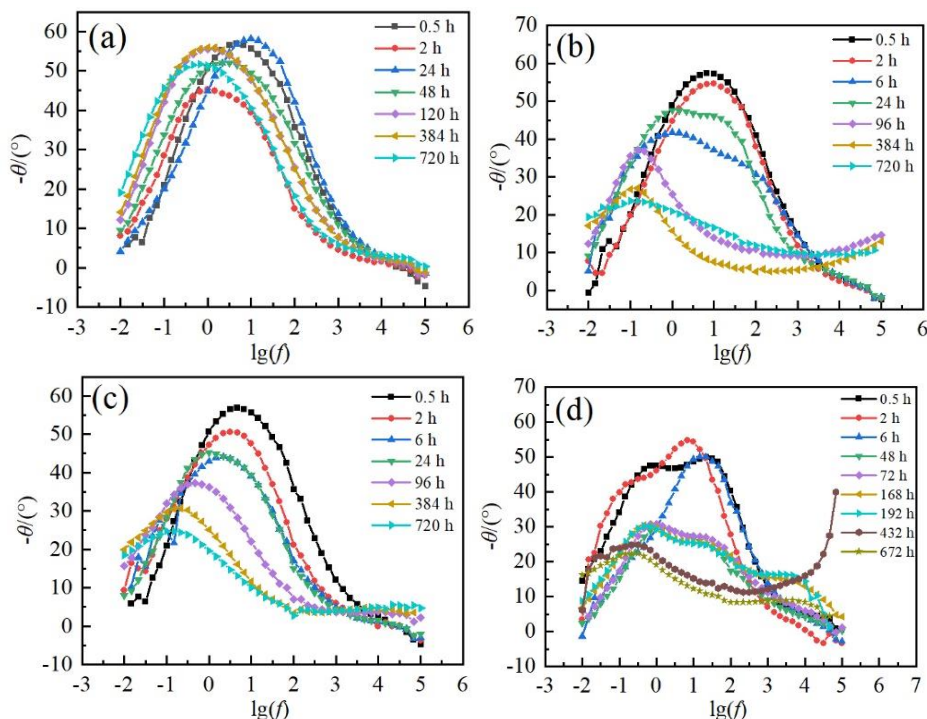
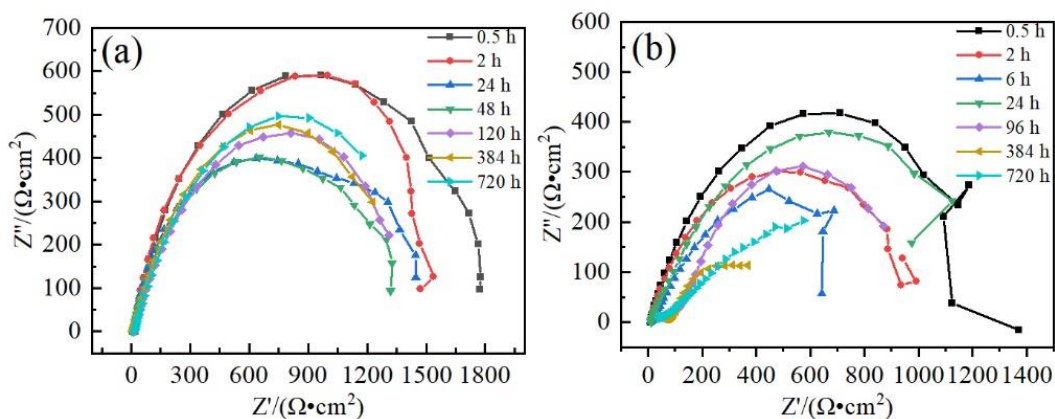


Figure 2. Bode diagram of hull steel erosion corrosion at different seawater flow rates: (a) 0 m/s, (b) 2 m/s, (c) 4 m/s, (d) 6 m/s



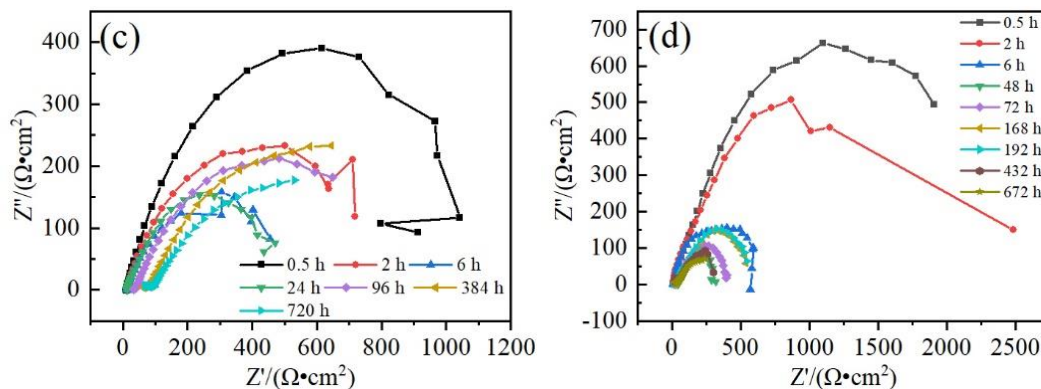


Figure 3. Nyquist diagram of hull steel erosion corrosion at different seawater flow rates: (a) 0 m/s, (b) 2 m/s, (c) 4 m/s, (d) 6 m/s

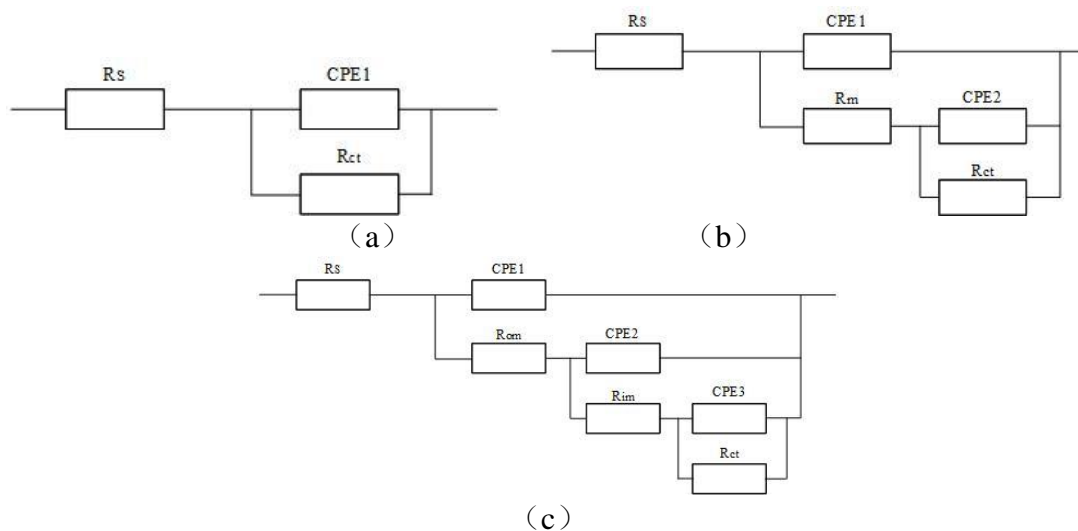


Figure 4. Equivalent circuit for fitting the electrochemical impedance spectrum

Corrosion characteristics of hull steel in different seawater flow rates after 30 days were analyzed by electrochemical impedance. Nyquist and Bode spectra of hull steel at different flow rates with time are shown in Fig. 2 and Fig. 3, respectively.

According to the characteristics of the peaks in the Nyquist and Bode diagrams in Fig. 2 and Fig. 3, the corresponding time-constant and corrosion characteristics can be determined. In the static state, the EIS spectrum of the first 48 hours is fitted the equivalent circuit diagram in Fig. 4(a) by Z-view software, and the equivalent diagram in Fig. 4(b) was used for the period of 72 -720 hours [39]. In the 2 m/s flow rate seawater, the corrosion process in the first 2 hours and 96-720 hours had a time constant, and 6-24 hours had two time-constants, the equivalent circuit diagrams of Fig. 4(a) and Fig.4(b) were used for fitting. In 4 m/s flowing seawater, the time-constant of the high frequency region of the EIS corresponds to the corrosion product film layer or the surface oxide film layer, and the time-constant of the medium and low frequency region corresponds to the corrosion reaction, which was fitted by the equivalent circuit diagram of Fig. 4(a) and Fig. 4(b). In the 6 m/s flowing seawater, the equivalent circuit diagrams of Fig. 4(a) and Fig. 4(c) were used for fitting. In the above equivalent circuit, CPE1 was the membrane capacitor, Rct was reaction resistance, Rs was the solution resistance, Rm was the membrane

resistance, CPE2 was the inner membrane capacitance, CPE3 was the reaction interface capacitance, R_{om} was the outer membrane resistance, and R_{im} was the inner membrane resistance.

In general, the charge transfer resistor R_{ct} was used to characterize the rate of corrosion [40]. The larger the reaction resistance, the smaller the electrochemical corrosion rate. According to the results of the above fitting, the change tendency of the reaction resistance of the hull steel during the 30 days corrosion process at different flow rates was obtained. The results were shown in Fig. 5(a). It can be seen that in the 0 m/s test, the charge transfer resistance R_{ct} value decreased rapidly within the first 24 hours, because it was difficult to form a passivation film on the steel surface, the corrosion rate increased. As the corrosion progresses until 216 hours, the corrosion product of the steel surface generated, the exposed area of the substrate in seawater was reduced, so the R_{ct} increased, the corrosion rate decreased. After 216 hours, the R_{ct} value was relatively stable with the extension of the corrosion time. The reason may be that the corrosion product covered the entire surface of the electrode, so the corrosion rate had not great change.

Under the 2 m/s flow rate test, in the first 425 hours' corrosion, R_{ct} continued to decrease with time, indicating that the corrosion rate increased first. This was possibly due to the rotating circle at a high speed, so the dissolved oxygen in the seawater rises, leading to the acceleration of the electrochemical corrosion. As the corrosion progressed until 500 hours, the corrosion product of the steel surface generated, so the R_{ct} increased, the corrosion rate decreased. When the test time was more than 500 hours, the R_{ct} was relatively stable at a small value. The reason for this may be that the product film formed by corrosion in flowing seawater was thin and the outer corrosion product film is loose and porous.

Under the 4 m/s flow rate test, in the first 25 hours' corrosion, the outer corrosion product film was difficult to form under the condition of 4 m/s high flow rate seawater flushing, the corrosion rate was accelerated, and the potential was rapidly negatively shifted. As the corrosion lasts until 150 hours, the inner layer corrosion product film is formed, the corrosion rate was slowed. When the corrosion time was more than 150 hours, the R_{ct} was relatively stable at a small value, and the formation and peeling of the local corrosion product film may cause an increase and decrease of the charge transfer resistance.

Under the 6 m/s flow rate test, the electrochemical corrosion rate rose rapidly within 6 hours. because it was difficult to form a dense passivation film on the electrode surface with a high content of aggressive particles Cl^- in the seawater at the beginning. As the corrosion progressed until 80 hours, the inner layer corrosion product film was formed, the corrosion rate was slowed. When the corrosion time is more than 80 hours, the R_{ct} was relatively stable.

Above all, the different flow rate corrosion R_{ct} during these 30 days, electrochemical corrosion rate expressed by charge transfer resistance undergoes rapid rise-slow down-gradual recovery to a stable process. And the time formed stable corrosion product film was becoming short with the flow rate increase, which was related to the dissolved oxygen in the water.

A large amount of corrosion products generated during the scouring process, which not only affected the diffusion of the corrosive medium on the surface of the substrate, but also protected the substrate from mechanical erosion. Therefore, when comparing the corrosion rates at the four flow rates, the charge transfer resistance and film resistance were fully considered, as well as the influence of factors such as solution resistance on corrosion. The reciprocal of the sum of the three can be used to characterize

the overall electrochemical corrosion rate precisely. The result was shown in Figure 5(b). In the first 2 hours of the initial corrosion, electrochemical corrosion accelerated as the seawater flow rate increased. With the increase of erosion time, the corrosion rates at 0 m/s, 2 m/s and 6 m/s flow rate remain basically unchanged within the first 120 hours, while the corrosion rate at 4 m/s flow rate decreased rapidly. After 120 hours, the corrosion rate of 0 m/s and 4 m/s seawater flow rate remain basically the same; the corrosion rates of 2 m/s and 6 m/s seawater flow rate increased rapidly; and when the flow rate was higher than 2 m/s, the electrochemical corrosion rate no longer increased or even decreased with the increase of the flow rate. Therefore, it was preliminarily determined that 2 m/s is the critical flow rate of erosion corrosion of hull steel in this corrosive environment.

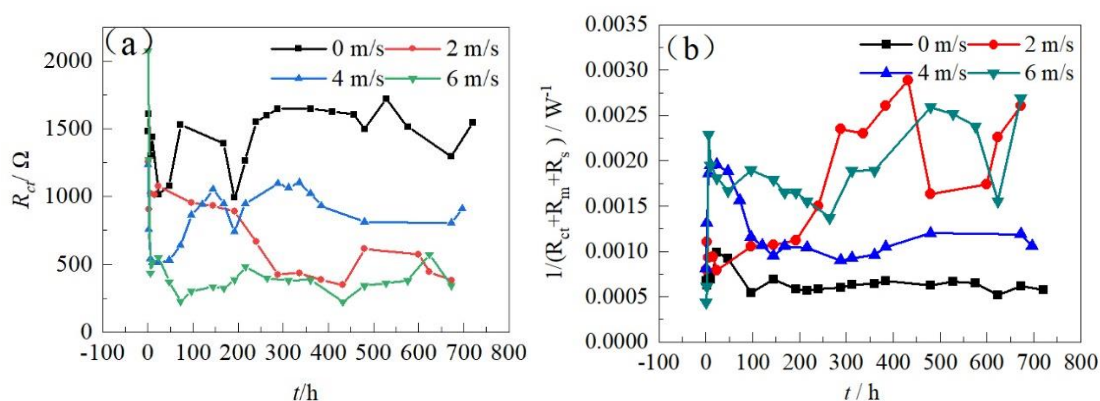


Figure 5. The variation of corrosion rate with time at different flow rates: (a) transfer resistance;(b) total resistance rate

3.3 Electrochemical noise

Fig.6 was a plot of potential noise over time at different points during 30 days of scouring corrosion. As shown in Fig. 6(a), the trend of static potential noise change can be divided into two stages. In the first stage (within 216 hours), the potential changed rapidly with time and became progressively smaller. The reason was that it was difficult for hull steel to form a stable passivation film in seawater. As the corrosion progresses, electrochemical corrosion was intensified; in the second stage (216-720 hours), the surface of the electrode was completely covered by corrosion products, especially the dense inner corrosion product film, the potential remains relatively stable.

As shown in Fig. 6(b), the trend of potential noise at the flow rate of 2 m/s can be roughly divided into two stages. In the first stage (0-216 hours), the potential shift negatively as the erosion corrosion progressed, indicating that electricity is generated, and the trend of chemical corrosion was enhanced; the potential of the second stage (216 -720 hours) first shift height, then maintain slight fluctuation and the range changed relatively stable than the beginning, indicating that the inner corrosion product film has formed rapidly and the electrochemical corrosion rate was stable.

As shown in Fig. 6(c), the trend of potential noise variation at the flow rate of 4 m/s can be divided into two stages. At the beginning of erosion corrosion, the potential dropped sharply as the erosion corrosion progressed, indicating that the erosion accelerated the corrosion of hull steel. Subsequently, although the potential fluctuates slightly, the range changes relatively stable than the

beginning, indicating that the inner corrosion product film had rapid formation and electrochemical corrosion rate was relatively stable.

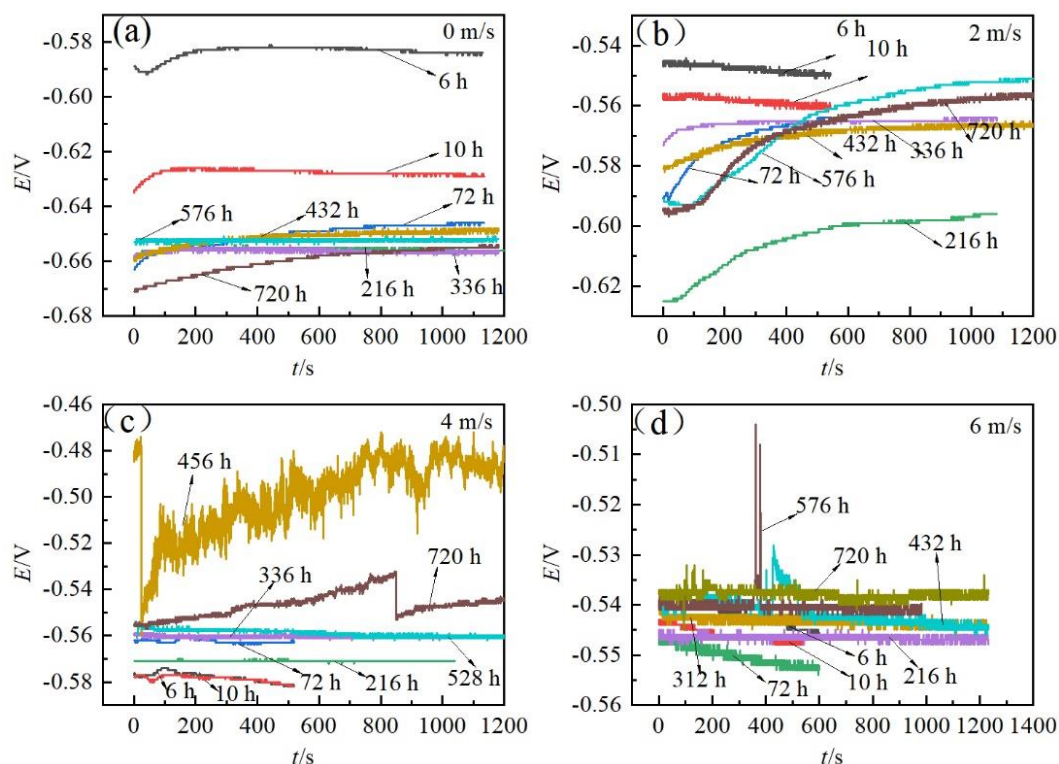


Figure 6. Electrochemical potential noise under different flow rates: (a) 0 m/s;(b) 2 m/s; (c) 4 m/s; (d) 6 m/s

As shown in Fig. 6(d), the trend of potential noise at 6 m/s flow rate shifts negatively with the increase of erosion time in the initial 72 hours, indicating that the electrochemical corrosion rate increased with time. After that, the potential remained substantially stable, and fluctuates as the surface corrosion products fall off and form.

In general, the trend of potential noise with time was consistent with the trend of Rct.

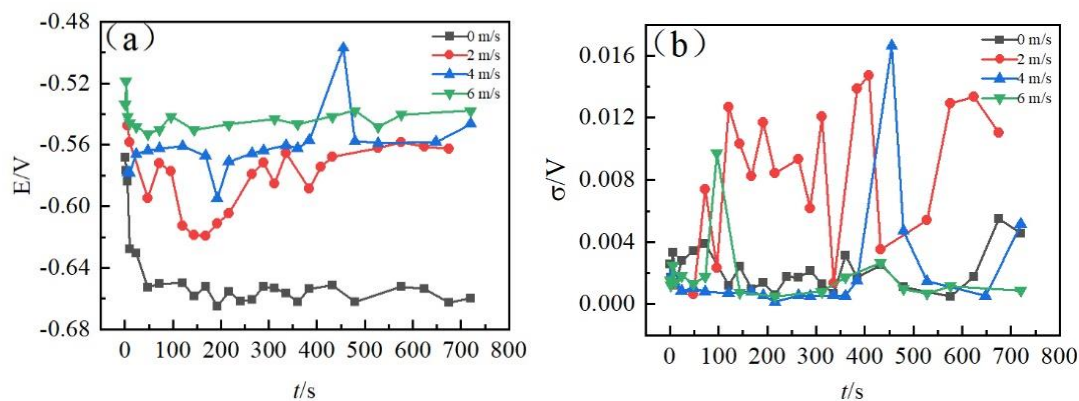


Figure 7. Electrochemical noise average potential and standard deviation: (a) average noise potential;(b) potential noise standard deviation

As shown in Fig. 7(a), as the flow rate increased, the average value of the electrochemical noise potential gradually increased, indicating that the corrosion trend was gradually increasing. As shown in Fig. 7(b), the standard deviation of the electrochemical noise potential under 2 m/s flow rate was the largest, indicating that in this flow rate the electrochemical reaction was most severe. Therefore, it can be further judged that 2 m/s is the critical flow velocity of the scouring corrosion of hull steel in the corrosive environment [41].

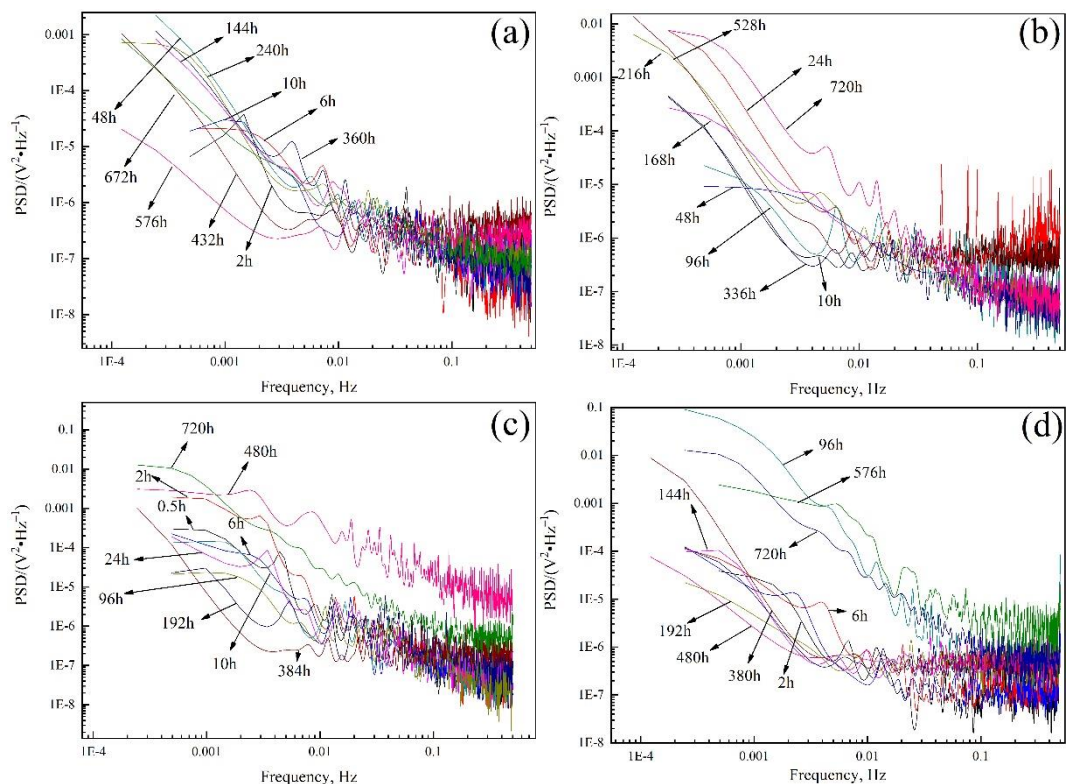


Figure 8. Electrochemical potential noise PSD spectrum under different flow rates: (a) 0 m/s; (b) 2 m/s; (c) 4 m/s;(d) 6 m/s

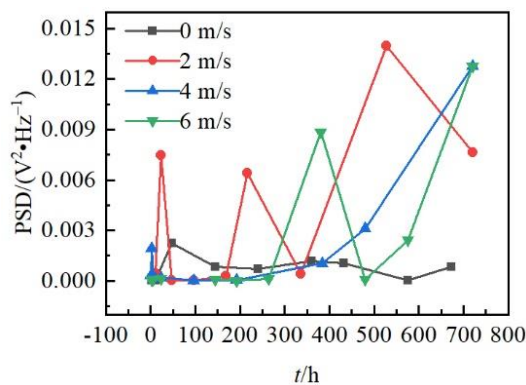


Figure 9. PSD white noise change of steel corrosion under different flow rates

The potential noise can be expressed as time functions, so a period of EN data can be converted into PSD spectrum by MEM [42]. The result was shown in Fig. 8. It can be seen that as the flow rate increased, the PSD curve gradually diverged, indicating that the trend of corrosion was gradually increasing. In Fig. 9, the white noise characteristic parameters of the PSD were calculated by fitting. It can be seen that the white noise value level and the fluctuation amplitude of the 2 m/s seawater flow rate were relatively largest, indicating that the corrosion rate was the largest at this flow rate. This also implies that 2 m/s flow rate was the critical speed.

3.4 SEM analysis

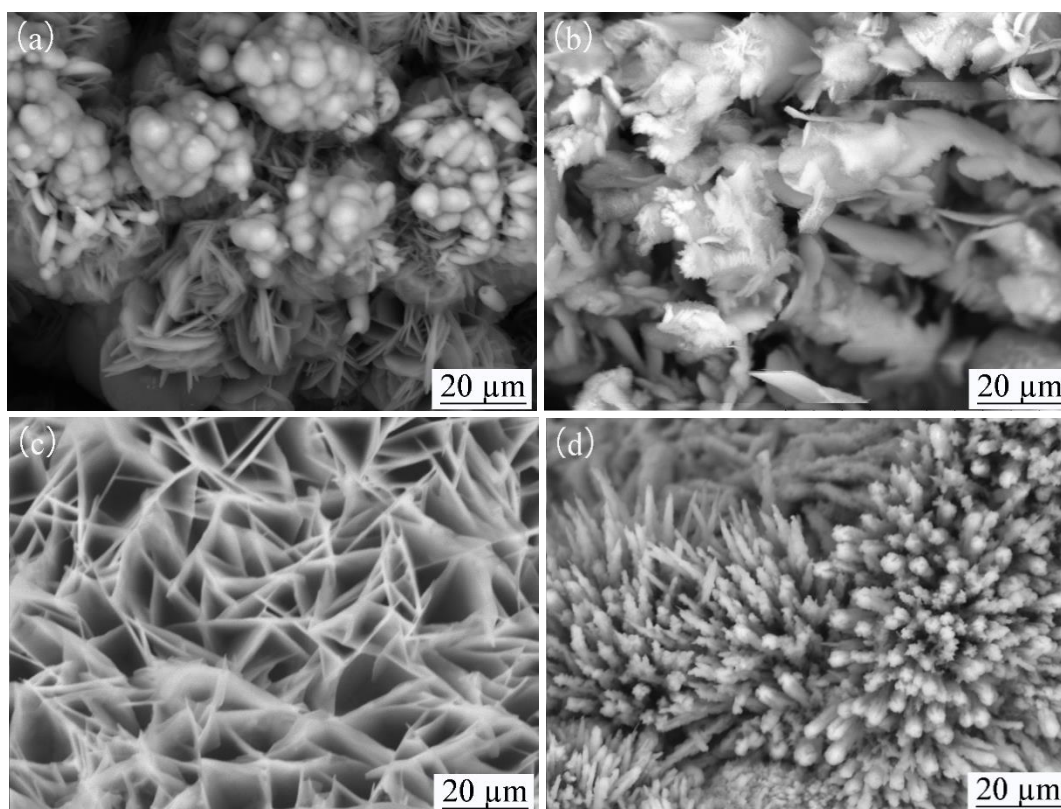


Figure 10. SEM photograph of hull steel after 30 days of erosion corrosion (a) 0 m/s;(b) 2 m/s; (c) 4 m/s; (d) 6 m/s

As shown in Fig. 10, the hull steel corroded in 0 m/s, 2 m/s, 4 m/s and 6 m/s flowing seawater after 30 days had different surface morphology. In static status, the corrosion product was similar to cauliflower (cluster), the surface of the electrode was completely covered by corrosion products, especially the dense inner corrosion product film. In 2 m/s flow rate, the surface of hull steel was obviously worse than that of static seawater. The dendritic or flaky structure of the corrosion product was more favorable for the transport of aggressive particles than the spherical structure of the former, and the electrochemical corrosion rate would become larger [43]. In 4 m/s flow rate, the product film basically has a network structure, indicating that the inner layer corrosion product was gradually transformed into a loose layer of outer layer. In 6 m/s flow rate, the needle-like corrosion product appears

on the surface, indicating that with the flow rate increased, the sheer force of the fluid and the surface of the substrate was increased, the shedding of the outer corrosion product was accelerated. Comparing the surface morphologies in these different conditions, it can be seen that the corrosion product of static corrosion was similar to cauliflower (cluster); the corrosion products on the surface of hull steel at 4 m/s and 6 m/s flow rate were net-like; and the corrosion products at 2 m/s flow rate were between the two. The structural characteristics of the corrosion products also prove that 2 m/s is the hull steel critical flow rate of erosion corrosion in this corrosive environment.

Through the above electrochemical impedance spectroscopy, electrochemical noise and SEM analysis, it can be comprehensively seen that 2 m/s was the critical flow rate. Therefore, in the future, this critical flow rate should be considered as an important operation parameter, it was best for the ship and pipe to avoid running at this speed.

4. CONCLUSIONS

In this paper, the critical flow velocity of hull steel was obtained for the first time by using a self-designed rotary erosion corrosion test platform. EIS, EN and SEM method were used to analyze the erosion corrosion characteristics in a 30-day long experiment. The following conclusions can be obtained:

(1) The higher the flow rate, the more complex the erosion corrosion synergy reacted. In each of the flow rate during these 30 days, electrochemical corrosion rate undergoes rapid rise- slow down-gradual recovery to a stable process, and the high flow rate may led to corrosion rate stable rapidly.

(2) With the increase of the flow velocity, the electrochemical noise average potential increased and the PSD curve gradually diverged. The 2 m/s flow rate electrochemical noise potential standard deviation and the white noise level had the largest value and fluctuation.

(3) As the flow rate increased, double-layer corrosion products generated; the outer corrosion products became thinner and the inner layer of corrosion products gradually formed; the corrosion product morphology at static was similar to cauliflower, while the morphology at 4 m/s and 6 m/s flow rate were net-like, and the morphology at 2 m/s flow rate were between them.

(4) Based on the experimental results and comprehensive analysis, the critical synergy velocity of hull steel erosion in the East China Sea can be determined as 2 m/s. This information was useful in the future to reduce erosion corrosion of hull steel and increase material service life.

References

1. F. Stott, J. Breakel, *Wear*, 135 (1989), 119.
2. J. Aguirre, M. Walczak, and M. Rohwerder, *Wear*, (2019), 438.
3. O.M. Irfan, and H.M. Omar, *Metall. Mater. Trans. A*, 50 (2019) 4232.
4. K. Selvam, A. Ayyagari, H.S. Grewal, S. Mukherjee, and H.S. Arora, *Wear*, (2017), 386.
5. G.T. Burstein, and K. Sasaki, *Wear*, 240 (2000) 80.
6. A. Neville, M. Reyes, and T. Hodgkiess, *Wear*, 238 (2000) 38.
7. L. Niu, and Y.F. Cheng, *Wear*, 265 (2008) 367.

8. Z.B. Zheng, and Y.G. Zheng, *Corros. Sci.*, 102 (2016) 259.
9. A. Neville, F. Reza, and S. Chiovelli, *Wear*, 259 (2005) 181.
10. B.R. Tian, and Y.F. Cheng, *Corros. Sci.*, 50 (2008) 773.
11. B.D. Jana, and M.M. Stack, *Wear*, 259 (2005) 243.
12. L. Zeng, S. Shuang, X.P. Guo, and G.A. Zhang, *Corros. Sci.*, 111 (2016) 72.
13. Y.H Wu, S.X Luo, and Q.S Mou, *Int. J. Electrochem. Sci.*, 15 (2020) 576.
14. L. Niu, and Y.F. Cheng, *J. Mater. Sci.*, 42 (2007) 8613.
15. J. Sun, C. Sun, G. Zhang, X. Li, W. Zhao, T. Jiang, H. Liu, X. Cheng, and Y. Wang, *Corros. Sci.*, 107 (2016) 31.
16. L. Majid, E.H. Anthony, and X. Wei, *Corros. Sci.*, 155 (2019) 67.
17. J.F. Flores, A. Neville, and N. Kapur, *Wear*, 267 (2009) 213.
18. J.K. Young, W.K. Su, and B.K. Han, *Corros. Sci.*, 152 (2016) 202.
19. D.W. Zhang, and X.P. Zhang, *Surf. Coat. Technol.* 190 (2005) 212.
20. B.T. Lu, J.F. Lu, and J.L. Luo, *Corros. Sci.*, 53 (2011) 1000.
21. Y.Z. Xu, and Y.J. Mike, *Corros. Sci.*, 139 (2018) 438.
22. M.C. Dai, X.B. Wan, and J.F. Qi, *Corros. Protect.*, 40 (2019) 479.
23. M. Sabrina, P. Nadine, and R. Sophie, *Electrochem. Acta.*, 87 (2013) 32.
24. H. Shahalia, H.M. Ghasemia, and M. Abedinib, *Corros. Sci.*, 233 (2019) 366.
25. M.M. Stack, and S.M. Abdelrahman, *Wear*, 273 (2011) 38.
26. M.M. Stack, N. Corlett, and S. Zhou, *Wear*, 203 (1997) 474.
27. L.F Cao, Z.B Qin, Y.Y Deng, C Zhong, W.B Hu, and Z Wu, *Int. J. Electrochem. Sci.*, 15 (2020) 628.
28. W.S. Peng, X.J. Liu, and S.T. Liu, *Surf. Technol.*, 48 (2019) 230.
29. M.M. Stack, and G.H. Abdulrahman, *Tribol. Int.*, 43 (2010) 1268.
30. Y. Chen, W.J. Kang, and M. Yao, *Corros. Sci.*, 40 (2019) 436.
31. C.G. Telfer, M.M. Stack, and B.D. Jana, *Tribol. Int.*, 53 (2012) 35.
32. S. Tao, and H. Huang, *Int. J. Electrochem. Sci.*, 14 (2019) 5435
33. H. Meng, X. Hu, and A. Neville, *Wear*, 263 (2007) 355.
34. R.O. Rihan, and S. Nesic, *Corros. Sci.*, 48 (2006) 2633.
35. X. Hu, and A. Neville, *Wear*, 258 (2005) 641.
36. Y.G. Zheng, Z.M. Yao, and X.Y. Wei, *Wear*, 186 (1995) 555.
37. Z.M. Yao, Y.G. Zheng, and W. Ke, *Wear*, 186 (1995) 568.
38. X.Q Fu, M.Q Shen, J.R Lin, X.S Wang, Q.Q Wang, and Y Xu, *Int. J. Electrochem. Sci.*, 15 (2020) 816.
39. J. Ouassira, H. Bennis, H. Benqliloub, M. Galaia, Y. Hassania, M.Ebn Touhamia, K. Berramib, And M. Lemyasser, *Colloids Surf.* 586 (2020) 124151.
40. C.A. Loto, and R.T. Loto, *Int. J. Electrochem. Sci.* 7 (2012) 12021.
41. F. Mansfeld, Z Sun, and C.H Hsu, *Corros. Sci.*, 43 (2001) 341.
42. A. Nagiub, F. Mansfeld, *Corros. Sci.*, 43 (2001) 2147.
43. J.R Jiang, Y.S Xie, M.A. Islam, and M. M. Stack, *J. Bio. Tribo. Corros.*, 3 (2017) 45.